European Polymer Journal 163 (2022) 110944

Contents lists available at ScienceDirect

European Polymer Journal

journal homepage: www.elsevier.com/locate/europolj

Promoted cellular uptake and intracellular cargo release of ICG/DOX-carrying hybrid polymeric nanoassemblies upon acidity-activated PEG detachment to enhance cancer photothermal/chemo combination therapy

Yu-Ning Hung [a], Yu-Ling Liu [a], Ya-Hsuan Chou [a], Shang-Hsiu Hu [b], Bill Cheng [c], Wen-Hsuan Chiang [a,*]

[a] Department of Chemical Engineering, National Chung Hsing University, Taichung 402, Taiwan
[b] Department of Biomedical Engineering and Environmental Science, National Tsing Hua University, Hsinchu 300, Taiwan
[c] Graduate Institute of Biomedical Engineering, National Chung Hsing University, Taichung 402, Taiwan

ARTICLE INFO

Keywords:
Indocyanine green
Photothermal/chemo therapy
Acidity-triggered dePEGylation
Controlled drug release
Hybrid polymeric nanoassemblies

ABSTRACT

Some studies have reported that the PEGylation of nanoparticle-based drug delivery systems could increase drug solubility, prolong systematic circulation time of drug carriers and decrease immunogenicity. Nevertheless, the uptake of these PEGylated nanoparticles by cancer cells was largely hindered. To promote intracellular co-delivery of indocyanine green (ICG), an amphiphilic photothermal transduction agent, and doxorubicin (DOX), a chemotherapy drug, for improved anticancer efficacy of the photothermal/chemo combination therapy, the hybrid polymeric nanoassemblies equipped with acid-activated PEG detachment were developed as vehicles by co-assembly of hydrophobic poly(lactic-co-glycolic acid) (PLGA), pH-responsive methoxy poly(ethylene glycol)-benzoic imine-octadecane ($mPEG_{5k}$-b-C_{18}) and amphiphilic tocopheryl polyethylene glycol succinate (TPGS) segments in aqueous solution of pH 8.0. The ICG/DOX-carrying $mPEG_{5k}$-b-C_{18}/TPGS/PLGA nanoassemblies (ID@PbCTPNs) were characterized to exhibit a well-dispersed spherical shape and maintained stable colloidal structure in serum-containing solution. Also ID@PbCTPNs sufficiently reduced ICG self-aggregation and leakage in pH 7.4 aqueous solution, thereby enhancing aqueous photostability and photo-elicited hyperthermia of ICG molecules. With the solution pH being lowered from 7.4 to 5.0, the acid-triggered dePEGylation of ID@PbCTPNs not only led to reduction of particle size but also accelerated cargo liberation. The findings of in vitro cellular uptake and cytotoxicity revealed that the cellular uptake and intracellular drug release of ID@PbCTPNs was appreciably increased via acid-elicited dePEGylation, thus largely promoting their anticancer potency on TRAMP-C1 cells by the photothermal/chemo combinatorial therapy. This work demonstrates that the designed ID@PbCTPNs show the promising application in cancer treatment.

1. Introduction

Cancer has been one of the most prevalent public health concerns in many countries of the world, showing that the cancer treatment relying on single therapeutic modality remains unsatisfying [1,2]. To promote therapeutic efficacy and minimize side effects, the combination therapy has emerged as a promising approach [2–6]. Importantly, it has been demonstrated that the combination of therapeutic strategies with various drugs and acting mechanisms can reverse multidrug resistance (MDR) of cancer cells and endow cancer cells sensitive to therapeutic agents [5–8]. Chemotherapy is one of the main clinical approaches of cancer treatment, but faces several limitations such as poor water solubility of drugs, unsatisfied pharmacokinetics and insufficient deposition of drug in tumor region and drug resistance [9,10]. As another main approach, the photothermal therapy (PTT) has been extensively adopted for cancer treatment due to its several advantages including little systemic side effect, the remote spatiotemporal control, precise and effective localized treatment [2,4]. In PTT application, the photosensitizers capable of generating hyperthermia by absorbing near infrared (NIR) light was utilized to ablate cancer cells [2,4,8]. Some studies disclosed that the integration of photothermal therapy (PTT) and chemotherapy can prominently boost anticancer potency by a synergistic effect

* Corresponding author.
E-mail address: whchiang@dragon.nchu.edu.tw (W.-H. Chiang).

https://doi.org/10.1016/j.eurpolymj.2021.110944
Received 2 October 2021; Received in revised form 6 December 2021; Accepted 9 December 2021
Available online 14 December 2021

[8,11–15]. PTT has been demonstrated to promote the tumor and cellular uptake of chemotherapy drugs by increasing the tumor vessel and cell membrane penetrability, and can reversal multidrug resistance mechanisms such as drug efflux [8,12,15].

Taking advantage of the enhanced permeability and retention (EPR) effect of tumor sites, a varied of nanoparticles capable of selectively co-delivering photothermal agents and chemotherapy drugs toward tumor tissues have been developed to effectively suppress tumor growth by photothermal/chemo combination therapy [11–16]. For example, Liu's group created a new theranostic Abraxane-like formulation composed of human serum albumin (HAS), paclitaxel (PTX), a hydrophobic chemotherapy drug, and indocyanine green (ICG), an amphiphilic photothermal agent, to effectively treat subcutaneous and metastatic breast tumors by combined PTT and chemotherapy under the guidance of NIR imaging [13]. Moreover, Cheng and co-workers developed poly (ethylene glycol) (PEG)-modified polydopamine nanoparticles (PDA-PEG) as vehicles of doxorubicin (DOX) and 7-ethyl-10-hydroxycamptothecin (SN38) [11]. The drug-loaded PDA-PEG showed not only well-controlled drug release in response to multiple stimuli including NIR light, pH and reactive oxygen species but also remarkable tumor growth inhibition in vivo by the combined PTT and chemotherapy.

Several studies pointed out that the PEGylation of polymeric nanoparticles could partly prolong their blood circulation time but remarkably hinder their cellular internalization and tumor accumulation, thus being not beneficial for tumor-targeted drug delivery [17–22]. To overcome the "PEG dilemma" on the impact of drug delivery, new strategies of equipping drug-loaded nanoparticles with detachable PEG shield in response to weak acidity (pH_e 6.2–7.0) and hypoxia of tumor microenvironment have been proposed [17–22]. For example, Tian's group synthesized a pH-sensitive polymer, PEG-benzoic imine-poly (γ-benzyl-l-aspartate)-b-poly(1-vinylimidazole) block copolymer (PPBV), to develop a pH multistage responsive micellar system for co-delivering PTX and curcumin [20]. The pH-responsive micelles intelligently switched the surface charge from neutral to positive, de-shielded the PEG layer and reduced particle size after long-circulation and extravasation from leaky blood vessels at tumor sites, thus facilitating their cellular uptake and deep tumor penetration to achieve superior tumor inhibition activity and effective breast cancer stem cells-killing capacity in vivo. Moreover, Guo and co-workers utilized a boric acid derivative, phenylboronic acid pinacol ester, as the hydrophobic moieties to form the reactive oxygen species (ROS)-responsive core loaded with DOX molecules and surrounded by azobenzene (azo)-containing PEG coating [21]. Once accumulated into the tumor upon EPR effect, the drug-carrying nanoparticles undergoing hypoxia-triggered PEG detachment via azo degradation exposed the tumor associate macrophages (TAMs)-targeting ligands and released DOX intracellularly, thus depleting TAMs effectively in vivo.

The fabrication of the aforementioned polymeric nanoparticles with stimuli-triggered dePEGylation, nevertheless, usually involves the use of complicate polymeric materials and multi-step procedures. Furthermore, to our knowledge, few studies on the development of the PEG detachable polymeric nanoassemblies as vehicles capable of promoting intracellular co-delivery of photothermal agent and chemotherapy drug have been reported. In this work, in order to enhance anticancer potency by effective intracellular delivery of photothermal/chemo combination therapy, the hybrid polymeric nanoassemblies decorated with acid-labile detachable PEG coating were created as carriers of ICG and DOX. Through the conjugation of methoxy-PEG_{5k}-CHO ($mPEG_{5k}$-CHO) with 1-octadecanamine upon formation of acid-labile benzoic imine bond, the $mPEG_{5k}$-benzoic imine-octadecane ($mPEG_{5k}$-b-C_{18}) was attained. The amphiphilic $mPEG_{5k}$-b-C_{18} and tocopheryl polyethylene glycol succinate (TPGS) segments were co-anchored at the surfaces of

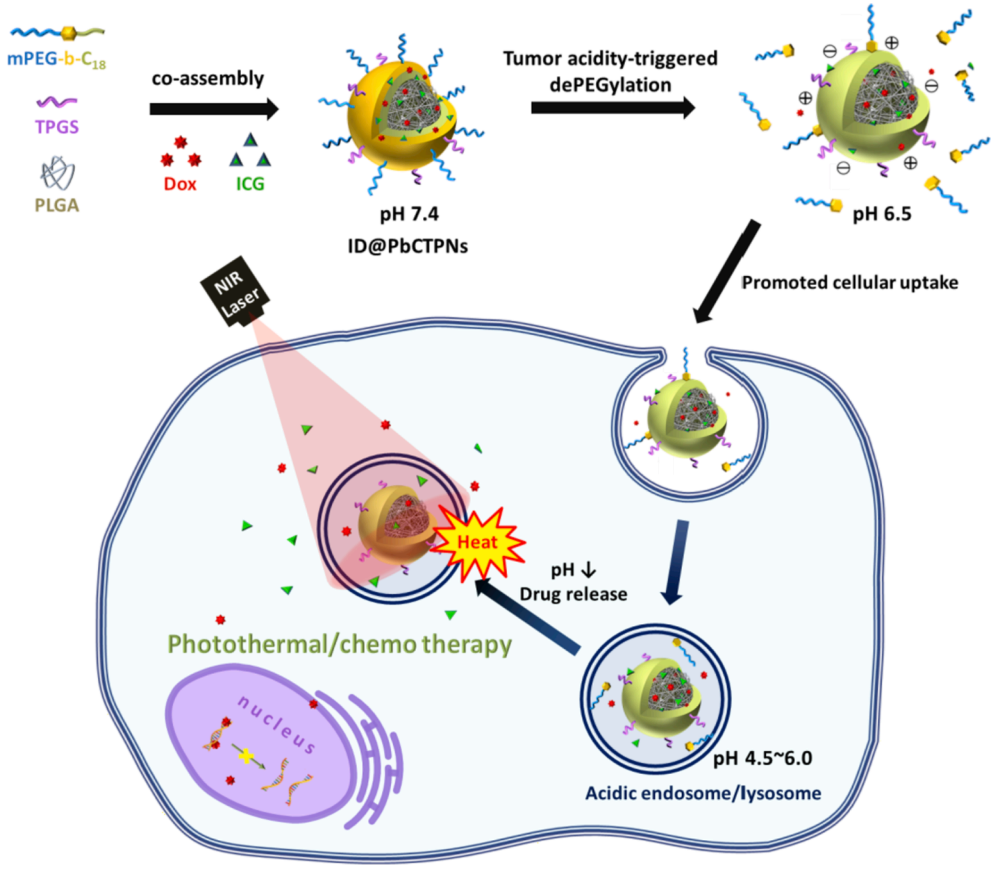

Scheme 1. Schematic illustration of the promoted cellular uptake and intracellular drug release of ICG/DOX-carrying hybrid polymeric nanoassemblies upon tumor acidity-triggered PEG detachment for enhanced cancer photothermal/chemo therapy.

ICG/DOX-carrying poly(lactic-co-glycolic acid) (PLGA) cores via the hydrophobic long-alkyl moieties (Scheme 1). In addition to the structural characteristics and NIR-triggered hyperthermia capability, the pH-triggered dePEGylation and in vitro drug release of ICG/DOX-loaded hybrid nanoassemblies were studied. Also the effects of acid-elicited dePEGylation on the cellular uptake of ICG/DOX-loaded hybrid nanoassemblies by TRAMP-C1 cells and their anticancer potency based on the combined PTT and chemotherapy were further evaluated.

2. Experimental section

2.1. Materials

Poly(ethylene glycol) methyl ether ($mPEG_{5k}$-OH, average Mn 5000), Dulbecco's modified Eagle's medium (DMEM, high glucose 4,500 mg/mL), Hoechst 33,342 (>98%) were purchased from Sigma-Aldrich (USA). 4-Dimethylaminopyridine (DMAP, 98%) and 4-formylbenzoic acid (FBA, 95+%) were obtained from Matrix Scientific. N,N′-dicyclohexylcarbodiimide (DCC, 99%) and 1-octadecylamine (97 %) were purchased from Alfa Aesar (USA). Stearic acid was obtained from Acros Organics. Poly(lactic-co-glycolic acid) (PLGA, lactide : glycolide = 75:25, IV 0.36 dL/g, acid-terminated) was purchased from Green Square (Taiwan). D-alpha-tocopheryl polyethylene glycol succinate (TPGS) and doxorubicin (DOX) hydrochloride were obtained from Carbosynth Ltd. (UK). Indocyanine green (ICG, 95.4%) was obtained from Chem-Impex (USA). Fetal bovine serum characterized (FBS, collected and processed in USA) was purchased from HyClone (USA). MTT ($C_{18}H_{16}BrN_5S$, > 98%) was obtained from ALPHA BIOCHEMSTRY (Taiwan). Deionized water was produced from Milli-Q Synthesis (18 MΩ, Millipore). All other chemicals were reagent grade and used as received. TRAMP-C1 cells (murine prostate cancer cell line) were obtained from Food Industry Research and Development Institute (Hsinchu City, Taiwan).

2.2. Synthesis of $mPEG_{5k}$-b-C_{18} and $mPEG_{5k}$-C_{18} adducts

The synthesis of $mPEG_{5k}$-benzoic imine-octadecane ($mPEG_{5k}$-b-C_{18}) based on Schiff base reaction of $mPEG_{5k}$-CHO and 1-octadecanamine was conducted according to our previous work [23]. The $mPEG_{5k}$-CHO utilized in this study was prepared as follow. First, $mPEG_{5k}$-CHO (521 mg, 1 equiv), 1-octadecanamine (32 mg, 1.2 equiv) and DMAP (24 mg, 2 equiv) were dissolved in dichloromethane (5.0 mL). After stirring at room temperature for 72 h, the solution was concentrated under reduced pressure. Next, the product was collected by precipitation from cold diethyl ether and dried under vacuum at 50 °C oven overnight. The synthetic procedure of $mPEG_{5k}$-b-C_{18} was presented in Scheme 2a. For comparison, the $mPEG_{5k}$-C_{18} without benzoic-imine bond was synthesized by Steglich esterification of $mPEG_{5k}$-OH and stearic acid (Fig. S1). The $mPEG_{5k}$-OH (500 mg, 1 equiv), stearic acid (57 mg, 2 equiv), DMAP

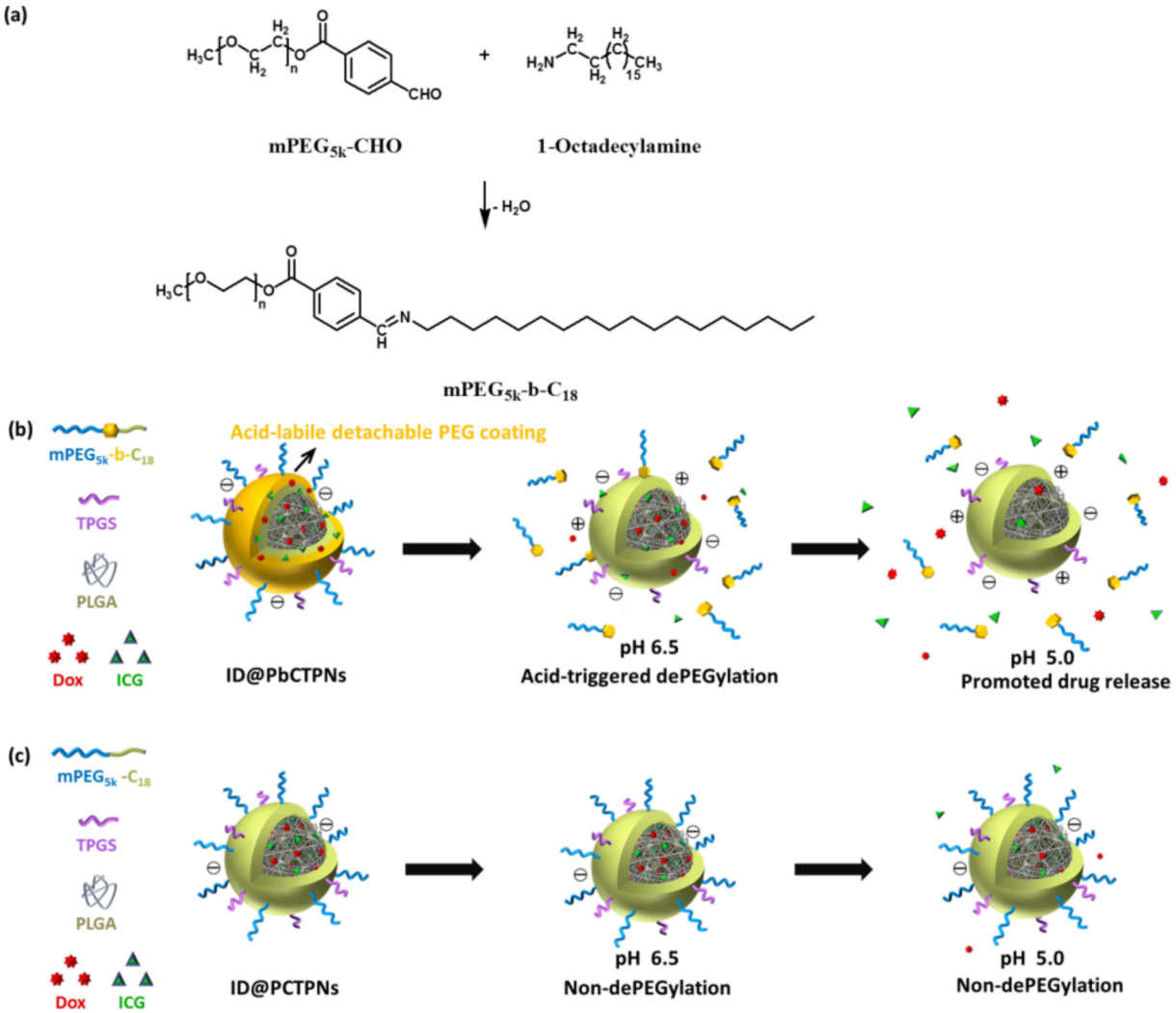

Scheme 2. (a) Synthetic route of $mPEG_{5k}$-b-C_{18}. (b) Scheme showing the structure of ID@PbCTPNs and their acid-triggered dePEGylation and drug release. (c) Scheme showing the structure of non-pH-responsive ID@PCTPNs.

(2.4 mg, 0.2 equiv) and DCC (41 mg, 2 equiv) were dissolved in dichloromethane (2.5 mL) sequentially. The reaction was carried out under stirring at room temperature for 24 h. After removal of the by-product N,N'-dicyclohexylurea, the solution was concentrated under reduced pressure. The white product was collected by precipitation from cold diethyl ether and dried under vacuum overnight. The chemical compositions of $mPEG_{5k}$-CHO, $mPEG_{5k}$-b-C_{18} and $mPEG_{5k}$-C_{18} were determined by Fourier transform infrared (FT-IR) spectrometer (FT-720, HORIBA) and proton nuclear magnetic resonance (^{1}H NMR) spectrometer (Agilent DD2 600 MHz NMR Spectrometer) using D_2O or $CDCl_3$ as the solvent.

2.3. Preparation of ICG/DOX-carrying hybrid polymeric nanoassemblies

In this study, various cargo-loaded hybrid polymeric nanoassemblies were fabricated by one-step nanoprecipitation method. For example, the ICG/DOX-loaded $mPEG_{5k}$-b-C_{18}/TPGS/PLGA nanoassemblies (ID@PbCTPNs) were prepared as follows. In brief, DMSO (0.4 mL) containing PLGA (4.0 mg), TPGS (0.5 mg), $mPEG_{5k}$-b-C_{18} (2.0 mg), ICG (0.2 mg) and DOX hydrochloride (0.2 mg) were added dropwise into the pH 8.0 phosphate buffer (0.01 M, 1.6 mL) under stirring. The mixture was stirred at room temperature for 16 h, following by equilibrium of additional 30 min. Next, the ID@PbCTPN suspension was dialyzed (MWCO 12–14 kDa) with phosphate buffer (pH 8.0, 0.01 M) at 4 °C for 24 h to remove DMSO and un-loaded drug. For comparison, ICG/DOX-loaded $mPEG_{5k}$-C_{18}/TPGS/PLGA nanoassemblies (ID@PCTPNs) and PLGA nanoassemblies (ID@PNs) were prepared in a similar approach.

2.4. Characterization of various hybrid polymeric nanoassemblies

The mean hydrodynamic diameter (D_h) and polydispersity index (PDI) of various hybrid polymeric nanoassemblies in aqueous solutions were determined by dynamic light scattering (DLS) using a Brookhaven BI-200SM goniometer equipped with a BI-9000 AT digital correlator using a solid-state laser (35 mW, $\lambda = 637$ nm) detected at a scattering angle of 90°. The data shown herein represent an average of at least triplicate measurements. To further explore the morphology of ID@PbCTPNs, ID@PCTPNs and ID@PNs dispersed in aqueous solution of pH 7.4, the angular dependence of the autocorrelation functions of various polymeric nanoassemblies was evaluated by the above apparatus. Also, the morphology of various cargo-loaded hybrid nanoassemblies with negative staining of 2 wt% phosphotungstic acid hydrate was examined by transmission electron microscope (TEM) (JEM-1400FLASH Electron Microscope, JEOL). The zeta potential of various hybrid polymeric nanoparticles was measured by a Particle Size Analyzer (Litesizer 500, Anton-Paar).

To quantify ICG and DOX encapsulated within nanoassemblies, a prescribed volume of payload-containing nanoassemblies solution was lyophilized and then dissolved in DMSO to extract the drug. The absorbance of ICG and DOX at 794 nm and 480 nm was determined, respectively, by a UV/Vis spectrophotometer (U-2900, Hitachi). Drug loading efficiency (DLE) and drug loading content (DLC) were calculated by the following equations:

$$\mathrm{DLE}(\%) = \frac{\mathrm{weightofdrugloaded}}{\mathrm{weightofdruginfeed}} \times 100\%$$

$$\mathrm{DLC}(\mathrm{wt}\%) = \frac{\mathrm{weightofdrugloaded}}{\mathrm{totalweightofdrug} - \mathrm{loadednanoparticles}} \times 100\%$$

To evaluate aqueous photo-stability of ICG, the characteristic ICG absorbance of various ICG-carrying nanoassemblies and free ICG (ICG concentration = 8 μM) in phosphate buffered saline (PBS, pH 7.4, 0.15 M) at 37 °C was determined over time by UV/Vis spectrophotometer (U-2900, Hitachi). The ICG absorbance (Abs) measured at different time intervals was normalized with the following formula.

$$\mathrm{Normalizedabsorbance}(\%) = \frac{\mathrm{Abs_{at\ different\ time\ intervals}}}{\mathrm{Abs_{at\ the\ beginning}}} \times 100\%$$

2.5. In vitro drug release study

For ICG release study, various ICG-loaded nanoassembly suspensions (1.5 mL) were dialyzed (Cellu Sep MWCO 12–14 kDa) against PBS (pH 7.4, 0.15 M) and acetate buffer saline (pH 5.0, 0.15 M) (30 mL) at 37 °C, respectively. The internal sample was taken out periodically for measurement of maximum ICG absorbance by the UV/Vis spectrophotometer (U-2900, Hitachi). The sample solution was then put back into the dialysis bag after each analysis. The cumulative ICG release (%) was obtained by the following formula:

$$\mathrm{CumulativeICGrelease}(\%) = \frac{A_0 - A_t}{A_0} \times 100\%$$

A_0 = Initial ICG absorbance

A_t = ICG absorbance at different time points

For DOX release assessment, the DOX-containing nanoassembly suspension (1.0 mL) was dialyzed (Cellu Sep MWCO 12–14 kDa) against PBS (pH 7.4, 0.15 M) and acetate buffered saline (pH 5.0, 0.15 M) (20 mL) at 37 °C, respectively, under gentle shaking (100 rpm). At different time intervals, 1.0 mL dialysate was taken for analysis and replaced with an equivalent volume of fresh buffer. The DOX fluorescence in the range 500–700 nm was determined by fluorescence spectrometer (F-2700, Hitachi) to obtain the amount of DOX released.

2.6. Temperature elevation under NIR laser irradiation

Free ICG and various ICG-loaded nanoassemblies in PBS (1.0 mL) were irradiated with 808 nm NIR laser (1.25 W/cm^2) for 5 min. During NIR laser irradiation, the solution temperature was measured by an infrared thermal imaging camera (Thermo Shot F30, AVIO). The temperature change of ID@PbCTPN solutions of different concentrations exposed to NIR laser irradiation was also monitored.

2.7. In vitro cellular uptake

TRAMP-C1 cells were cultured in high glucose DMEM medium containing penicillin-streptomycin solution (100 unit/L), sodium bicarbonate ($NaHCO_3$, 2.2 g) and 10 % FBS in 5% CO_2 at 37 °C. TRAMP-C1 cells (2×10^5 cells/well) were seeded in 6-well plate and cultured for 24 h. In order to explore the effect of acid-triggered dePEGylation of ID@PbCTPNs on their cell uptake, the ID@PbCTPNs were dispersed in PBS of pH 7.4 or 6.5 (acid pretreatment) at 37 °C for 3 h. Afterward the hybrid nanoassemblies were diluted with cell culture medium. TRAMP-C1 cells (2×10^5 cells/well) seeded in 6-well plate containing 22 mm round glass coverslips were incubated with the ID@PbCTPNs (DOX concentration = 10 μM) with acid pretreatment or not at 37 °C for 2 and 4 h. After being washed twice with PBS and fixed with 4 % formaldehyde, the cells were stained with Hoechst 33,342 for 15 min. The cellular uptake was observed by confocal laser scanning microscopy (CLSM) (FluoView FV3000, OLYMPUS) at the excitation wavelengths of 405 and 488 nm for Hoechst and DOX, respectively. For comparison, the internalization of ID@PCTPNs and ID@PNs with either acid pretreatment or not by TRAMP-C1 cells was also observed by CLSM.

2.8. In vitro cytotoxicity

To evaluate the effects of acid-triggered dePEGylation of ID@PbCTPNs on their DOX-mediated anticancer capability, the ID@PbCTPNs were pre-incubated in PBS of pH 7.4 or 6.5 at 37 °C for 3 h and then diluted with cell culture medium. TRAMP-C1 cells (1×10^4 cells/well) seed in a 96-well plate were incubated with ID@PbCTPNs receiving acid pretreatment or not for 24 h. Next 100 μL of MTT (0.25

mg/mL) was added into each well to dissolve the precipitate and the absorbance of resulting solution at 570 nm was determined by a microplate reader (800 TS, BioTek). For comparison, the cytotoxicity of PbCTPNs, PCTPNs, ID@PCTPNs, ID@PNs, free ICG and DOX was also studied by the same way.

To further assess the therapeutic efficacy of DOX chemotherapy integrated with ICG-mediated NIR-triggered PTT, TRAMP-C1 cells (2×10^5 cells/well) seeded in 6-well plate were incubated with various nanoparticles carrying either single- or dual-modality therapy (ICG concnetration = 0.4 μM, DOX concentration = 0.63 μM) with acid pretreatment or not for 16 h. After being washed twice with PBS, cells were detached with trypsine-EDTA and collected by centrifugation. The cell pellets suspended in 100 μL DMEM were irradiated with 808 nm NIR laser (1.25 W/cm^2) for 5 min. The laser-treated cells were reseeded in a 96-well plate and incubated for another 24 h. The cell viability was examined by the aforemented MTT assay. On the other hand, the anticancer activity of single PTT provided by I@PbCTPNs was explored by Hoechst/PI staining. After being incubated with I@PbCTPNs receiving either acid pretreatment or not for 24 h, TRAMP-C1 cells (1×10^5 cells/well) in a 12-well plate were exposed to irradiation of 808 nm NIR laser (1.25 W/cm^2) for 5 min at a selected area. Subsequently, the cells were doubled stained with PI and Hoechst 33342, and the cellular images were obtained using a NIB-100F inverted fluorescent biological microscope (Nanjing Jiangnan Novel Optics Co., Ltd., China).

2.9. Statistical analysis

All data are presented as the mean ± standard deviation (SD). Data analyses for two groups were performed using Student's *t*-test. Statistical significance is indicated as (n.s.) $P > 0.05$, (*) $P < 0.05$, (**) $P < 0.01$ and (***) $P < 0.001$.

3. Results and discussion

3.1. Synthesis and characterization of mPEG$_{5k}$-b-C$_{18}$ and mPEG$_{5k}$-C$_{18}$

According to our previous study [23], the mPEG$_{5k}$-CHO employed in this work was prepared by the coupling of mPEG$_{5k}$-OH with *p*-formylbenzoic acid. As shown in Fig. 1a and b, compared to the FT-IR spectrum of mPEG$_{5k}$-OH, the FT-IR spectrum of mPEG$_{5k}$-CHO exhibited the absorption bands at 1637 and 1712 cm^{-1} for C=O stretching vibration of aldehyde and ester groups, respectively. Moreover, different from the ^{1}H NMR spectrum of mPEG$_{5k}$-OH (Fig. 2a), the appearance of

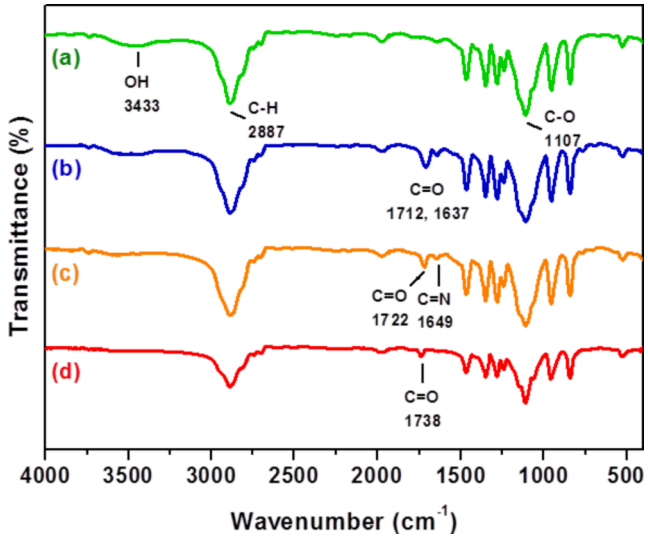

Fig. 1. FT-IR spectra of (a) mPEG$_{5k}$-OH, (b) mPEG$_{5k}$-CHO, (c) mPEG$_{5k}$-b-C$_{18}$ and (d) mPEG$_{5k}$-C$_{18}$.

feature proton signals of benzene ring at δ 8.1 and 8.3 ppm, and of aldehyde group at δ 10.1 ppm was observed in the ^{1}H NMR spectrum of mPEG$_{5k}$-CHO (Fig. 2b). These results confirm the effective conjugation of mPEG$_{5k}$-OH and *p*-formylbenzoic acid. Based on the signal integral ratio of the aldehyde protons (δ 10.1 ppm) and methoxy protons (δ 3.4 ppm) of mPEG$_{5k}$-CHO, the coupling efficiency beyond 94 % was attained. Next the mPEG$_{5k}$-b-C$_{18}$ with benzoic-imine bond was synthesized upon Schiff base reaction between aldehyde of mPEG$_{5k}$-CHO and primary amine of 1-octadecanamine. The appearance of a new absorption band at 1649 cm^{-1} from C=N stretching vibration was observed in the FT-IR spectrum of mPEG$_{5k}$-b-C$_{18}$ (Fig. 1c). Also, the ^{1}H NMR spectrum of mPEG$_{5k}$-b-C$_{18}$ (Fig. 2c) showed the complete vanishing of the proton signals of aldehyde group at δ 10.1 ppm and the presence of proton signals of aliphatic alkyl group at δ 0.9–1.2 ppm, and of imine bond at δ 8.3 ppm. The above findings strongly suggest the successful conjugation of mPEG$_{5k}$-CHO and 1-octadecanamine. The conjugation efficiency was estimated to be ca. 93 % based on the integral ratio of the methyl and methoxy proton signals of mPEG$_{5k}$-b-C$_{18}$. Importantly, in the ^{1}H NMR spectrum (Fig. 2e) of mPEG$_{5k}$-b-C$_{18}$ segments suffered from acid treatment, the proton signals of imine group significantly disappeared, while the proton signals of aldehyde group at δ 10.1 ppm appeared, suggesting the complete hydrolysis of the benzoic-imine linker under acidic condition.

For comparison, the mPEG$_{5k}$-C$_{18}$ lacking benzoic-imine bond was synthesized through the DCC/DMAP-mediated esterification of mPEG$_{5k}$-OH with stearic acid. The ^{1}H NMR spectrum of mPEG$_{5k}$-C$_{18}$ was presented in Fig. 2d. According to the integration ratio of the signals from the terminal methyl protons (δ 0.9 ppm) of stearic acid and methoxy protons (δ 3.4 ppm) of mPEG$_{5k}$, the coupling efficiency of ca. 98 % was estimated. Considering the hydrophilic nature of mPEG$_{5k}$ and hydrophobic property of 1-octadecanamine and stearic acid, the attained mPEG$_{5k}$-b-C$_{18}$ and mPEG$_{5k}$-C$_{18}$ adducts were expected to exhibit amphiphilic character, thus being able to anchor on the PLGA particles by the hydrophobic long alkyl groups to stabilize these nanoassemblies in aqueous solution with mPEG segments.

3.2. Preparation and characterization of ICG/DOX-encapsulated PLGA-based nanoassemblies

In this study, through the hydrophobic association of ICG and DOX molecules with PLGA segments in pH 8.0 aqueous solution, the ID@PNs were attained. In a similar way, the ID@PbCTPNs were fabricated by the coating of amphiphilic pH-sensitive mPEG$_{5k}$-b-C$_{18}$ segments and TPGS on the surfaces of ID@PNs upon hydrophobic anchor mechanism. For comparison, the ID@PCTPNs with surface coating of non-pH-responsive mPEG$_{5k}$-C$_{18}$ and TPGS were also prepared. Notably, compared ID@PNs (ca. 102 nm), the ID@PbCTPNs and ID@PCTPNs in pH 7.4 PBS exhibited somewhat larger particle size (Table S1 and Fig. 3a), being ascribed to the presence of the additional surface coating layer [23–25]. Note that, in the absence of TPGS, the co-assembly of mPEG$_{5k}$-b-C18 and PLGA segments tended to form quite large and unstable particles. This implies that the hydrophobic co-anchor effect of amphiphilic mPEG-b-C18 and TPGS on the surfaces of PLGA-based nanoparticles plays an important role in promoting colloidal stability, although the orientation of these molecules on molecular level is currently not clear. As shown in Fig. 3b, for ID@PbCTPNs and ID@PCTPNs, in addition to the feature absorption peak of DOX at 480 nm, the significant red shift of characteristic ICG absorption peak from 778 to 803 nm was observed, indicating the successful incorporation of DOX and ICG into these nanoassemblies. Similar loading efficiency and capacity of DOX and ICG were obtained for ID@PbCTPNs and ID@PCTPNs (Table S1).

To get insight into the structural characterization of cargo-loaded nanoparticles, the variable angle DLS and TEM measurements were conducted. As presented in Fig. 3c and d, a high linear relationship between the relaxation frequency (Γ) and the square of the scattering vector (q^2) was obtained for ID@PbCTPNs and ID@PCTPNs, indicating

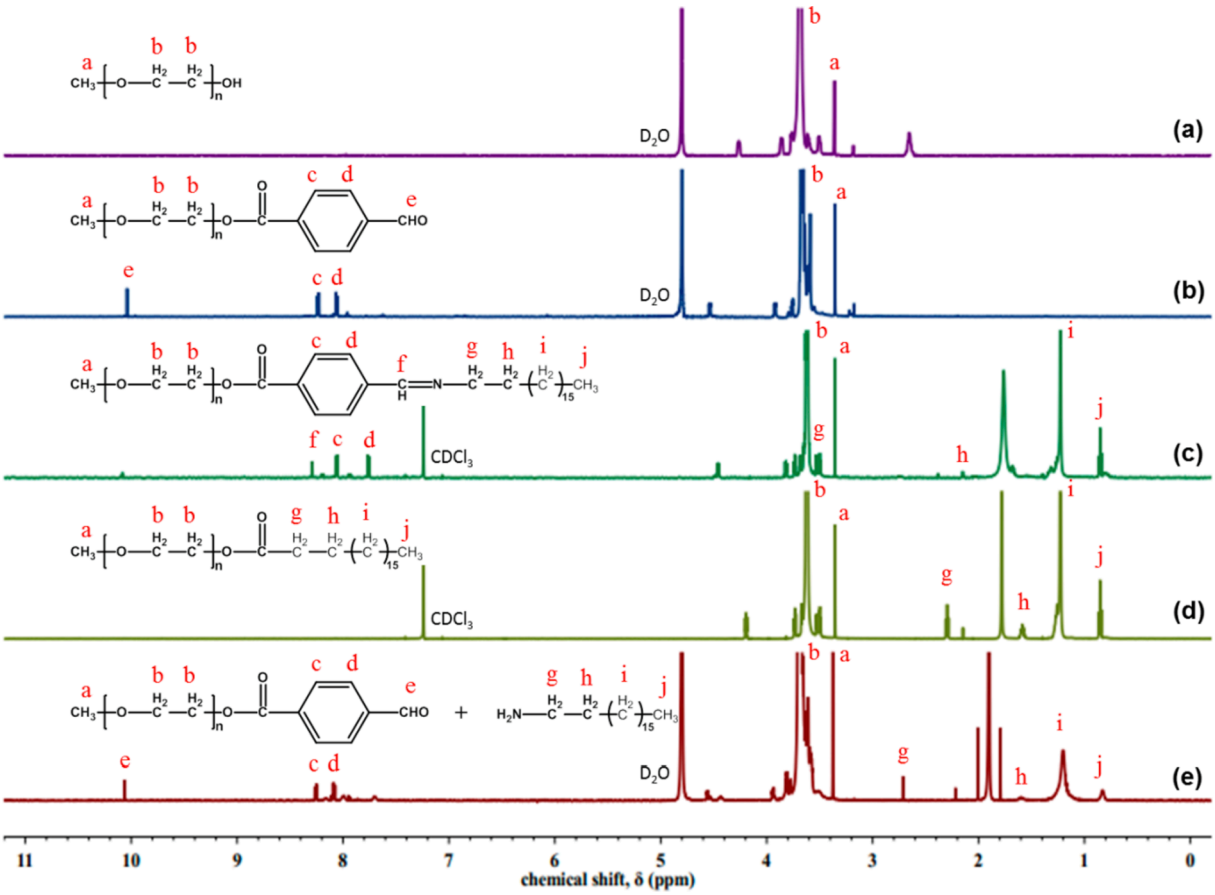

Fig. 2. ^{1}H NMR spectra of (a) $mPEG_{5k}$-OH, (b) $mPEG_{5k}$-CHO, (c) $mPEG_{5k}$-b-C_{18}, (d) $mPEG_{5k}$-C_{18} and (e) acid-treated $mPEG_{5k}$-b-C_{18}.

these nanoassemblies in a spherical form [26,27]. The well-dispersed spherical shape of ID@PbCTPNs and ID@PCTPNs was also observed in their TEM images (Fig. 3e and f). Note that the particle sizes of these cargo-loaded nanoassemblies observed by DLS were somewhat larger than those measured by TEM owing to their structural transition from swollen (DLS) to dehydration (TEM) status.

3.3. Acidity-triggered dePEGylation and in vitro cargo release

Notably, the zeta potential values of the ID@PbCTPNs and ID@PCTPN dispersed in aqueous solution of pH 7.4 were significantly lower compared to those of ID@PNs under the same milieu (Fig. 4a). This suggests that the PEG-rich surface coating of the ID@PbCTPNs and ID@PCTPNs can shade numerous negative charges from sulfonate groups of ICG molecules anchoring on PLGA cores. Similar findings regarding the sheltering of surface charges of various functionalized nanoparticles by their PEG-constituted shells have been also reported elsewhere [17,28]. Besides, at pH 7.4, the somewhat higher zeta potential (-12.1 mV) of ID@PbCTPNs compared to that (−4.7 mV) of ID@PCTPNs was attained. This could be ascribed to that the π-π stacking and hydrophobic interaction of amphiphilic ICG molecules with benzene ring-containing $mPEG_{5k}$-b-C_{18} segments during co-assembly could allow some of ICG molecules be entrapped within the surface benzoic imine-rich coating layer of ID@PbCTPNs, thereby partly declining the sheltering effect of $mPEG_{5k}$ segments on the negative charges (Scheme 2b). In contrast, due to the lack of benzene ring in $mPEG_{5k}$-C_{18}, most of ICG molecules were apt to hydrophobically anchor on the surfaces of PLGA cores of ID@PCTPNs (Scheme 2c). As a result, the outer $mPEG_{5k}$ segments could effectively shield the negative charges of ICG molecules.

When the solution pH was adjusted from pH 7.4 to 5.0, in addition to slightly reduced particle size from 143.2 to 131.2 nm (Fig. 4b), conversions in zeta potentials of ID@PbCTPNs from slightly negative (-12.1 mV) to nearly neutral values (-4.0 mV) were observed (Fig. 4a), clearly illustrating that the acid-activated hydrolysis of benzoic imine bonds remarkably facilitated the $mPEG_{5k}$-CHO detachment and protonation of primary amine groups from 1-octadecanamine (Scheme 2b). By contrast, no significant variation in particle size and zeta potential of ID@PCTPNs was attained in response to the pH adjustment to 5.0, indicating the lack of dePEGylation due to the absence of acid-labile linkages in $mPEG_{5k}$-C_{18} coating. It is worthy to notice that the ID@PbCTPNs undergoing partial dePEGylation maintained a well-dispersed colloidal structure when exposed to the weak acidic (pH 6.2) milieu near pH_e (Fig. 4b), an essential prerequisite for the promoted cellular uptake by cancer cells.

As revealed in Fig. 4c, different from quick diffusion of free ICG molecules through the dialysis tube in pH 7.4 aqueous solution (beyond 90 % within 6 h), the remarkable decline in cumulative ICG release (below 40 %) from ID@PbCTPNs and ID@PCTPNs was attained within 12 h. Similar results was also observed for ID@PNs (Fig. S2). This indicates that the hydrophobic PLGA matrix as physical barrier could retard leakage of ICG molecules to some degree. Note that, when the solution pH was changed from 7.4 to 5.0, the cumulative ICG release (over 80 % within 24 h) of ID@PbCTPNs was appreciably higher than that (about 50 %) of ID@PCTPNs. Also the considerably accelerated DOX release of ID@PbCTPNs in response to the pH reduction to 5.0 as compared with that of ID@PCTPNs was observed (Fig. 4d). These results suggest that the acid-elicited $mPEG_{5k}$-CHO detachment from coating layer of ID@PbCTPNs could impair the π-π stacking and hydrophobic interactions of nanoparticles with ICG and DOX payloads, thus promoting drug outflow (Scheme 2b). Tian's group also found that the acid-induced PEG-CHO separation from the PTX/curcumin-loaded pH multistage responsive micelles appreciably facilitated drug liberation

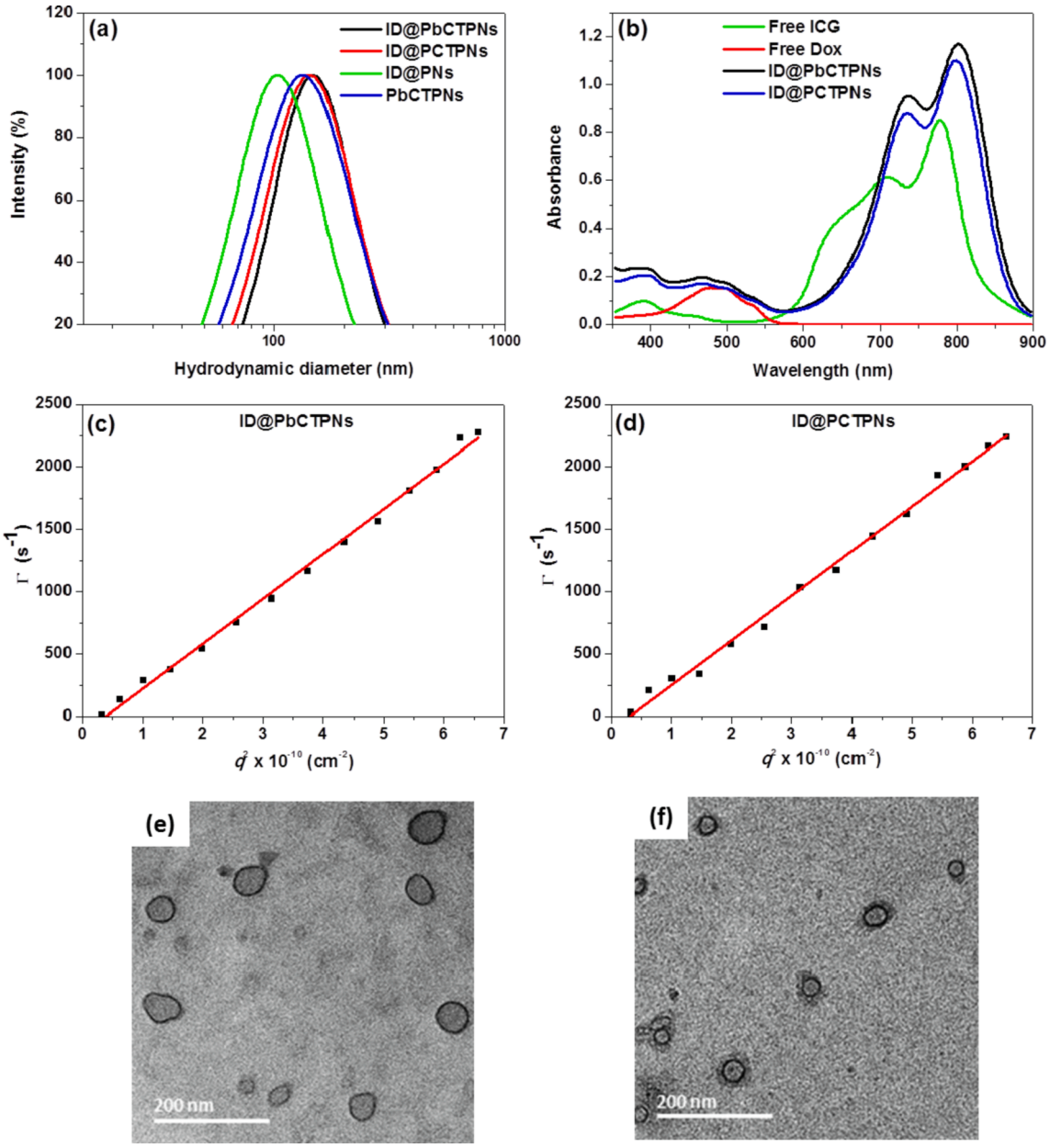

Fig. 3. (a) DLS size distribution profiles and (b) UV/Vis spectra of various cargo-loaded nanoassemblies in PBS. Angle-dependent correlation of Γ versus q^2 of (c) ID@PbCTPNs and (d) ID@PCTPNs in PBS. TEM images of (e) ID@PbCTPNs and (f) ID@PCTPNs. Scale bars are 200 nm.

[20]. Furthermore, the pH-triggered drug release of functionalized vehicles was reported elsewhere [29,30].

3.4. Optical and colloidal stability and photothermal behavior of cargo-loaded nanoassemblies

Notably, different from a significant reduction in the normalized absorbance of free ICG molecules in PBS over a period of 7 days, a little changed normalized absorbance of various ICG-carrying nanoparticles was attained (Figs. 5a and S3). A massive precipitation of free ICG in PBS was also observed within 24 h (Fig. S3). For ICG-loaded nanoassemblies, such an enhanced photostability was primarily attributed to the protective effect of PLGA cores employed as ICG dispersion matrices that effectively prevented rapid self-aggregation and degradation of ICG molecules in aqueous solutions [12,31,32]. Furthermore, these cargo-loaded nanoparticles maintained essentially unvaried particle size in pH 7.4 PBS at 37 °C within 7 days (Fig. 5b) and in 10 % FBS-containing PBS during 48 h (Fig. 5c), revealing their superior colloidal stability.

To evaluate the feasibility of ID@PbCTPNs used as PTT reagent, their NIR-induced photothermal conversion capability was determined by monitoring the solution temperature with an infrared thermal imaging camera. As shown in Fig. 5d and S4, under irradiation of 808 nm NIR laser, compared to PBS without appreciable temperature change, the aqueous solutions of free ICG and ICG-carrying nanoassemblies exhibited considerable temperature elevation due to the ICG-mediated photothermal effect. Note that, at the same irradiation time, the temperature increase of various ICG-encapsulated nanoassembly solutions was higher than that of free ICG solution. This is because the absorption of ICG inserted on the surfaces of PLGA nanoassemblies undergo red-shift (from 778 to 803 nm) to approach the central wavelength (808 nm) of the diode laser utilized, thus enhancing the photothermal conversion activity [12,33]. Furthermore, under NIR laser irradiation, the temperature variation profiles of ID@PbCTPNs and ID@PCTPNs in PBS were similar to that of ID@PNs. The photothermal

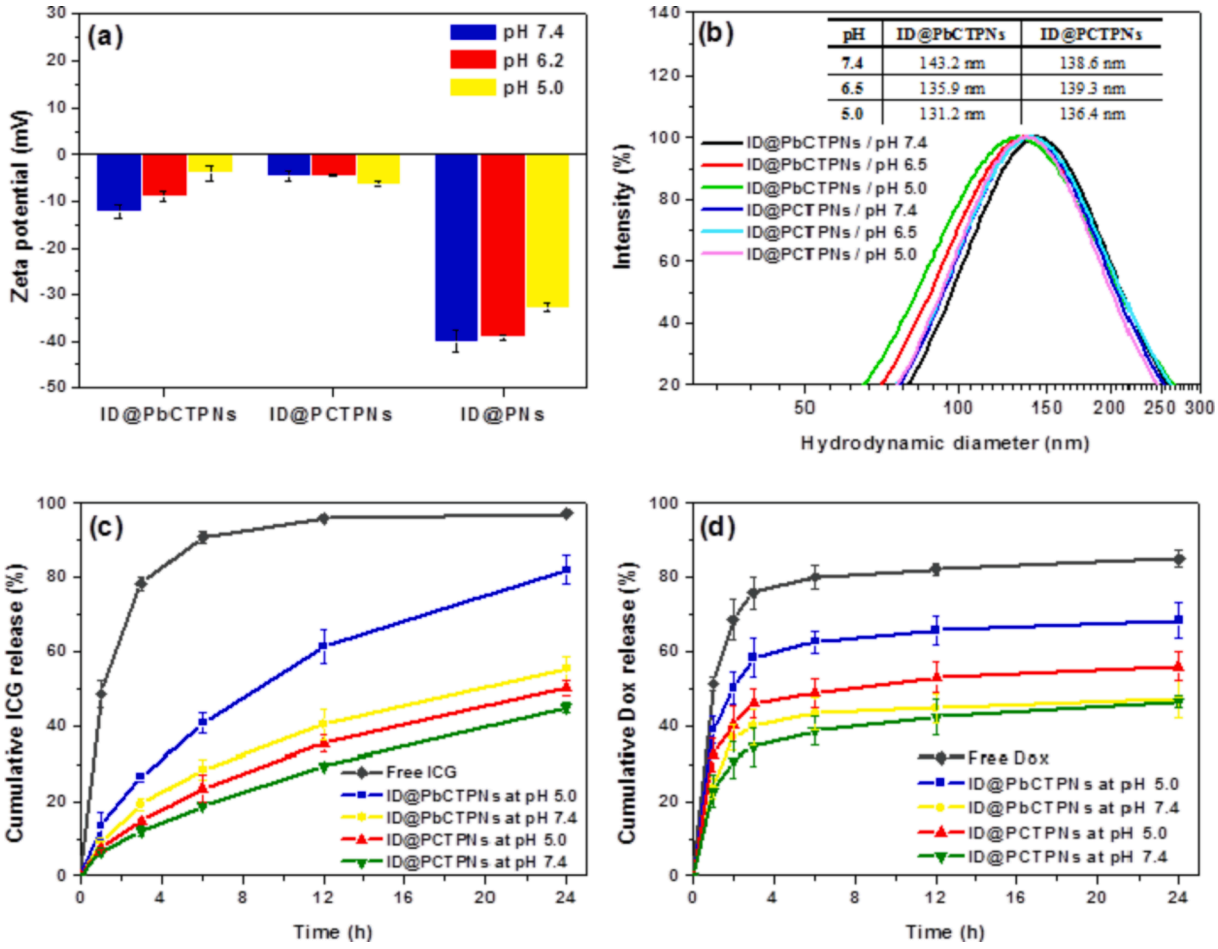

Fig. 4. (a) Zeta potential and (b) DLS particle size distribution profiles of various cargo-carrying nanoassemblies in aqueous solutions of different pH. (c) Cumulative ICG release profiles of ID@PbCTPNs and ID@PCTPNs in aqueous solutions of pH 7.4 and 5.0 at 37 °C. For comparison, diffusion of free ICG through the dialysis tube in pH 7.4 aqueous phase is included. (d) Cumulative DOX release profiles of ID@PbCTPNs and ID@PCTPNs in aqueous solutions of pH 7.4 and 5.0 at 37 °C. For comparison, diffusion of free DOX through the dialysis tube in pH 7.4 aqueous phase is included.

conversion efficiencies of ID@PbCTPN, ID@PCTPNs and ID@PNs were attained to be ca. 11.3, 11.5 and 14.8 %, respectively. These results evidently suggest that the surface coating layer of hybrid nanoassemblies could not impair the NIR-triggered hyperthermia performance of ICG molecules. Also, as expected, when the ICG concentration was increased from 5 to 20 μM, the temperature rise of ID@PbCTPN solution during NIR laser irradiation was further increased (Fig. S5). Interestingly, after 808 nm laser irradiation, the above ICG-containing nanoparticles exhibited slightly reduced particle size (Fig. S6), being possibly ascribed to some cargo release driven by NIR-triggered hyperthermia.

3.5. *In vitro cellular uptake*

In order to investigate the effects of the acid-triggered dePEGlation of ID@PbCTPNs on their cellular uptake, the CLSM images of TRAMP-C1 cells incubated with ID@PbCTPNs suffered from acid pretreatment or not were obtained. As shown in Fig. 6a, with 2-h incubation, TRAMP-C1 cells incubated with the acid-pretreated ID@PbCTPNs exhibited visible DOX fluorescence signals in comparison with the cells exposed to ID@PbCTPNs without acid pretreatment. With the incubation time being prolonged from 2 to 4 h, DOX delivered by the acid-pretreated ID@PbCTPNs was found appreciably in the nuclei of TRAMP-C1 cells as compared to the counterparts lacking acid pretreatment (Fig. 6b). Also, after receiving acid pretreatment, the ID@PbCTPNs enhanced intracellular DOX fluorescence intensity of TRAMP-C1 cells by 1.3 fold (Fig. 6c). By contrast, no significant difference in the DOX fluorescence intensity of TRAMP-C1 cells treated with ID@PCTPNs with and without acid pretreatment was observed post 4-h co-incubation. Importantly, with acid pretreatment, the ID@PbCTPNs showed the enhanced fluorescence intensity of DOX within the nuclei of TRAMP-C1 cells in comparison with ID@PCTPNs. The results evidently demonstrate that the acid-triggered dePEGylation of ID@PbCTPNs could not only enhance their internalization by TRAMP-C1 cells but also promote intracellular DOX release, thus facilitating translocation of DOX to cell nucleus. Similar findings that the functionalized drug-encapsulated polymeric nanoparticles considerably enhanced intracellular cargo delivery by the stimuli-triggered dePEGylation have been reported elsewhere [17,19,34].

Note that TRAMP-C1 cells treated with acid-pretreated ID@PbCTPNs showed significantly stronger DOX fluorescence signals compared to cells exposed to ID@PNs with and without acid pretreatment. Apparently, in addition to the acid-activated PEG detachment, the nearly neutral and TPGS-containing surfaces of ID@PbCTPNs partly augmented their cellular uptake, whereas the negative charges-rich surfaces of ID@PNs remarkably retarded their cellular internalization due to the repulsion force between the nanoassemblies and cell membranes. On the other hand, with 4-h incubation, the quite strong DOX fluorescence was observed in the nuclei of TRAMP-C1 cells exposed to free DOX molecules in comparison with that of cells incubated with all DOX-carrying nanoassemblies used in this work, being most likely attributed to the different cellular uptake pathways between free DOX

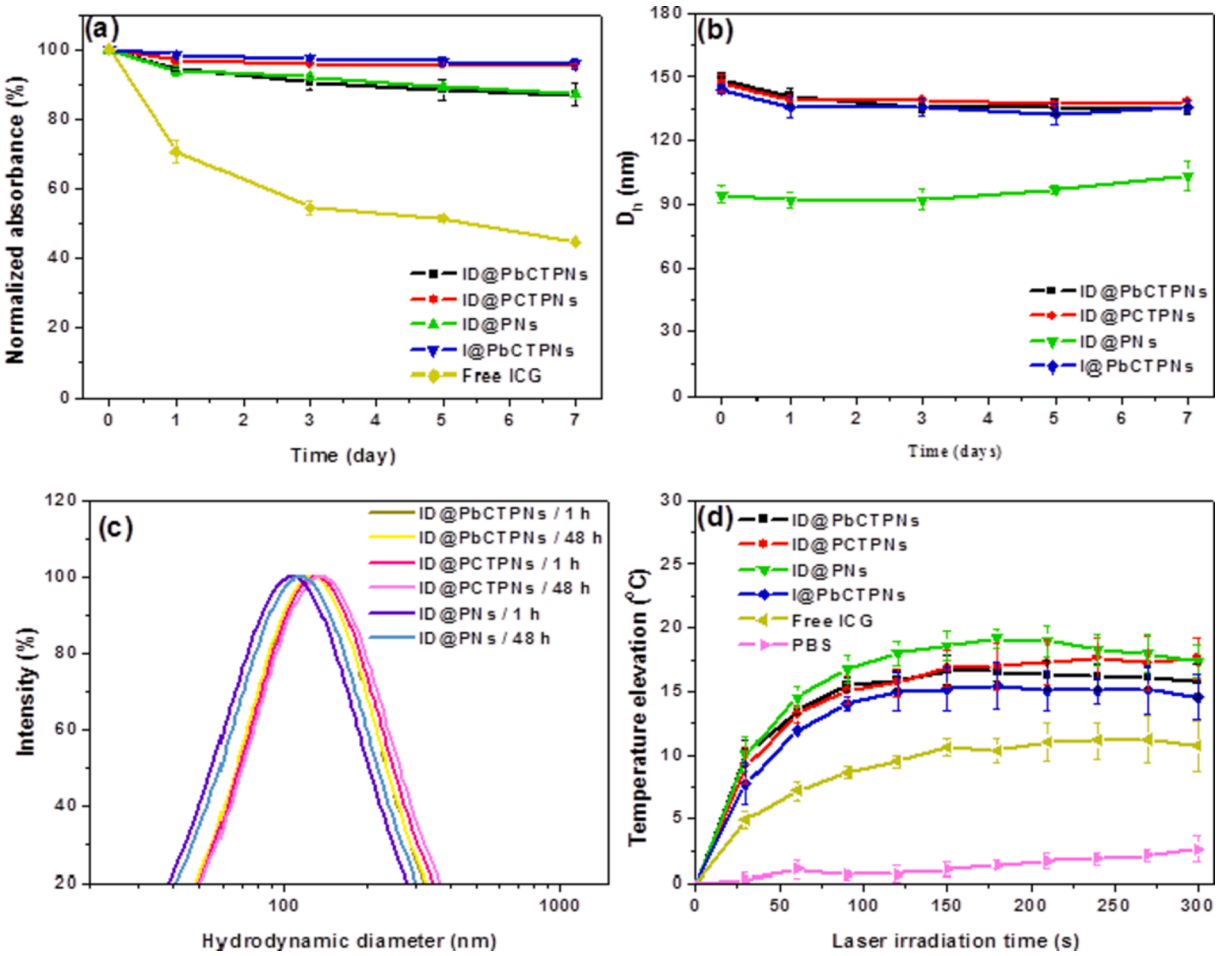

Fig. 5. (a) Normalized maximum absorbance of free ICG and various ICG-carrying nanoassemblies in pH 7.4 PBS at different time intervals. (b) Time-evolved mean hydrodynamic diameters (D_h) of various cargo-loaded nanoassemblies in PBS at 37 °C. (c) DLS particle size distribution profiles of ICG/DOX-loaded nanoassemblies dispersed in 10 % FBS-containing PBS at different time intervals. (d) Temperature change profiles of free ICG and various ICG-loaded nanoassemblies in PBS (ICG concentration = 10 μM) under irradiation of 808 nm NIR laser (1.25 W/cm^2).

(passive diffusion) and DOX-carrying nanoassemblies (endocytosis process) [35–37].

3.6. *In vitro photothermal/chemo combination therapy*

To explore the effects of acid-triggered dePEGylation of ID@PbCTPNs on their anticancer efficacy, we tested the viability of TRAMP-C1 cells receiving ID@PbCTPNs with either acid pretreatment or not by MTT assay. TRAMP-C1 cells incubated with drug-free PbCTPNs as a control group maintained the viability over 90 % (Fig. S7), indicating the non-toxicity of PbCTPNs to cancer cells. As shown in Fig. 7a, in the lack of NIR laser irradiation, compared to relatively high viability (ca. 90 %) of TRAMP-C1 cells treated with free ICG in the concentration range 0–3.2 μM, the viability of TRAMP-C1 cells exposed to free DOX was appreciably reduced with increased DOX concentration, suggesting the cytotoxic effect of DOX molecules. Notably, Fig. 7b revealed that the viability of TRAMP-C1 incubated with acid-pretreated ID@PbCTPNs was remarkably declined in comparison with that of cells receiving ID@PbCTPNs without acid pretreatment. This strongly demonstrates that the anticancer potency of acid-pretreated ID@PbCTPNs was prominently boosted through their promoted intracellular DOX transport driven by acid-elicited dePEGylation. In contrast, due to the absence of PEG detachment in response to acid pretreatment, the ID@PCTPNs with and without acid pretreatment displayed the similar DOX-mediated cytotoxicity on TRAMP-C1 cells (Fig. 7c).

Unexpectedly, regardless of acid pretreatment or not, compared to ID@PbCTPNs, the ID@PCTPNs showed higher anticancer capability, being probably resulted from some toxicity of drug-free PCTPNs against TRAMP-C1 cells (Fig. S7). Furthermore, the similar cytotoxicity of ID@PNs with and without acid pretreatment on TRAMP-C1 cells was attained (Fig. 7d). More importantly, with acid pretreatment, the drug dose required for 50 % cellular growth inhibition (IC_{50}) (0.96 μM) by ID@PbCTPNs was appreciably lower than that (3.55 μM) by ID@PNs. In view of the results of in vitro cellular uptake and cytotoxicity studies, it can be concluded that, in comparison with ID@PNs possessing highly negatively-charged surfaces, the ID@PbCTPNs suffered from acid-triggered dePEGylation exhibit nearly neutral and TPGS-containing surfaces, thus promoting cellular uptake and intracellular DOX liberation to considerably boost DOX-mediated anticancer efficacy. Also, as shown in the fluorescence staining of live/dead TRAMP-C1 cells (Fig. S8), with NIR laser irradiation, most of TRAMP-C1 cells incubated with acid-pretreated I@PbCTPNs presented PI-positive staining in comparison with cells treated with the counterparts without acid pretreatment, further proving that the enhanced intracellular ICG delivery by I@PbCTPNs upon acid-activated PEG detachment led to extensive cell death upon ICG-mediated PTT.

To further evaluate the anticancer effect of photothermal/chemo combination therapy delivered by ID@PbCTPNs, we determined the viability of TRAMP-C1 cells treated with ID@PbCTPNs plus NIR irradiation. As shown in Fig. 8a, the viability of TRAMP-C1 cells incubated with ID@PbCTPNs receiving acid pretreatment or not was further reduced by additional NIR irradiation. Also, regardless of acid

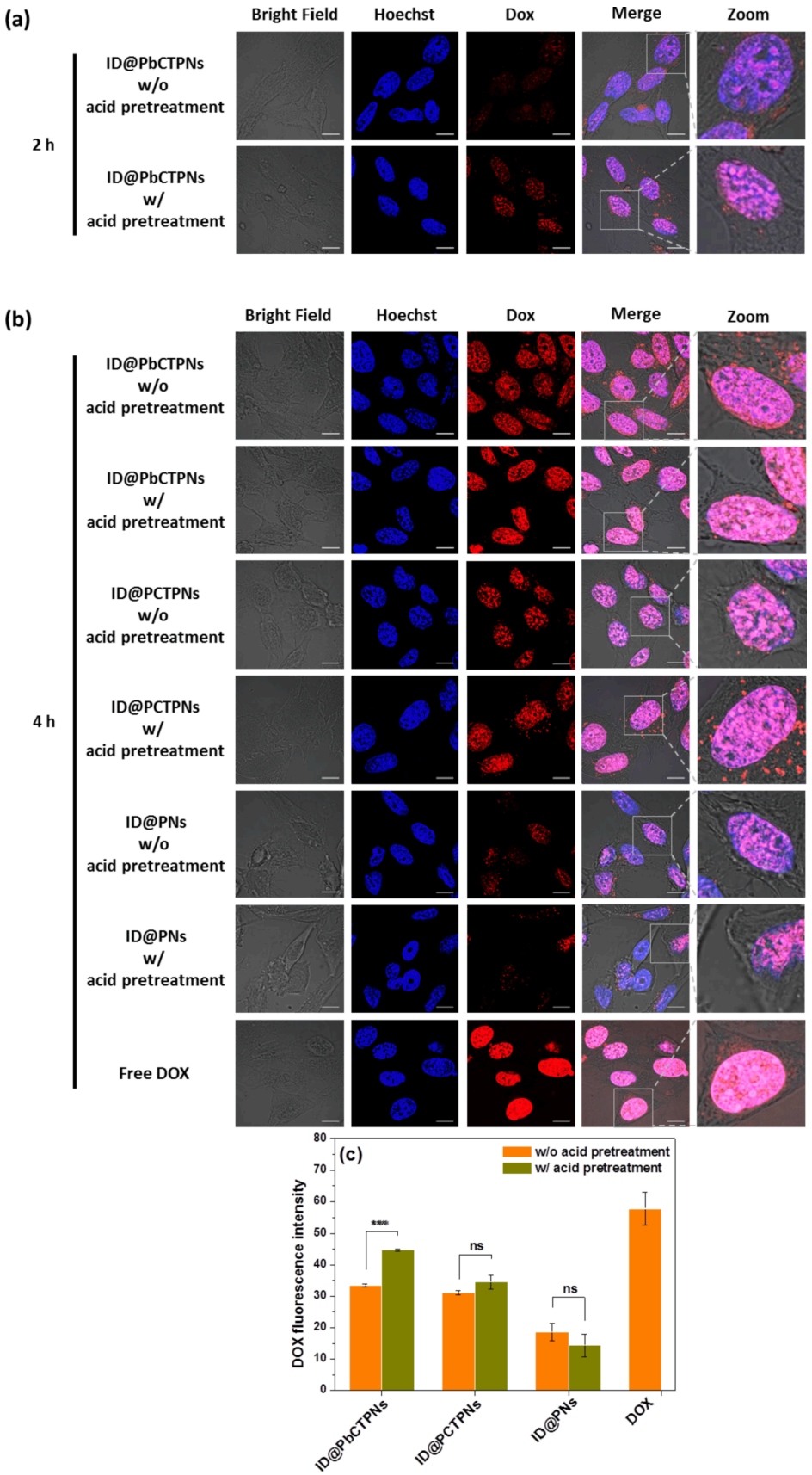

Fig. 6. (a) CLSM images of TRAMP-C1 cells exposed to ID@PbCTPNs with and without acid pretreatment for 2 h. (b) CLSM images and (c) quantified DOX fluorescence intensity of TRAMP-C1 cells treated with various cargo-loaded nanoassemblies with and without acid pretreatment for 4 h. Scale bars are 10 μm.

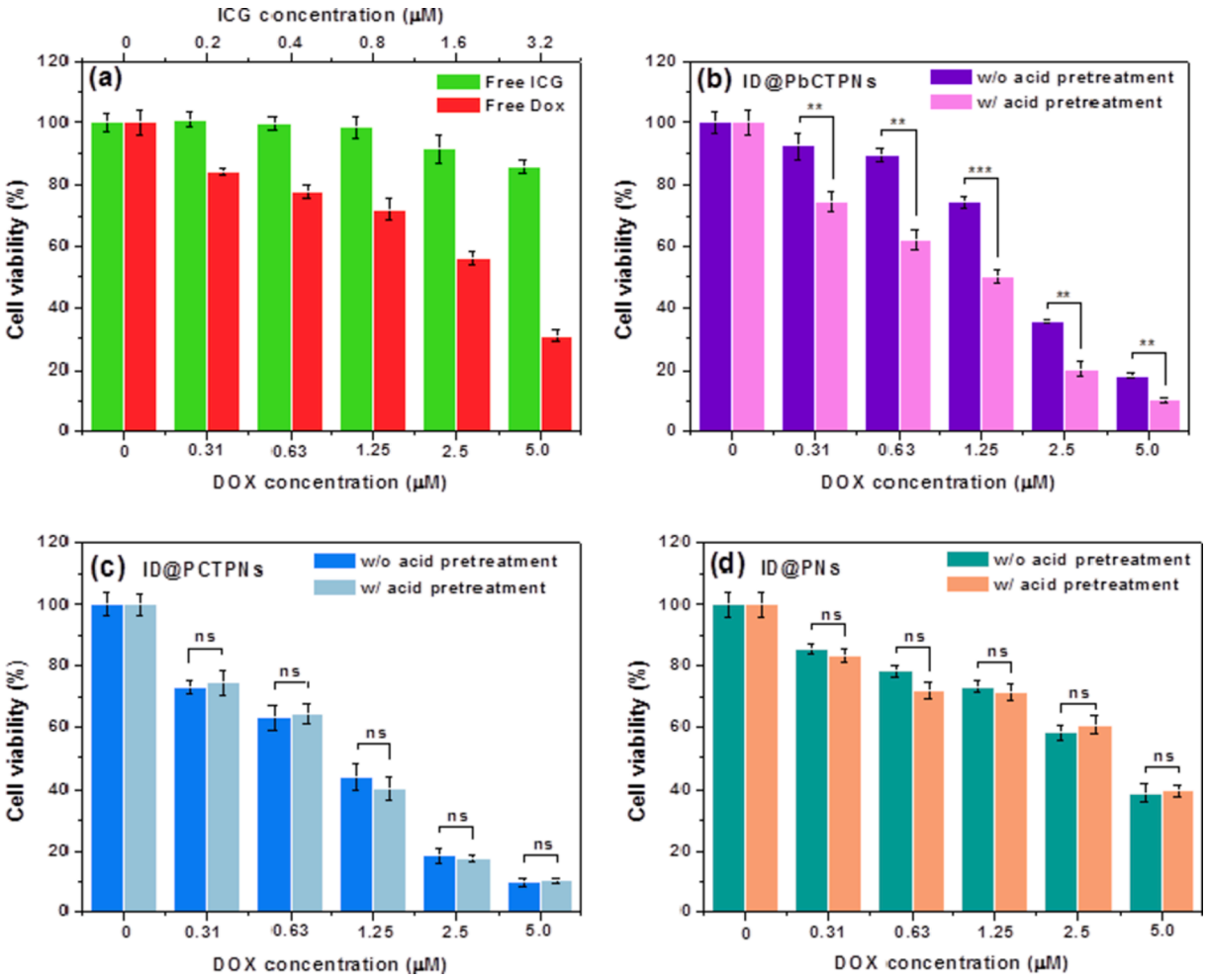

Fig. 7. (a) Viability of TRAMP-C1 cells incubated with free ICG and DOX, respectively, for 24 h in the lack of NIR laser irradiation. (b) Viability of TRAMP-C1 cells exposed to ID@PbCTPNs with and without acid pretreatment for 24 h in the lack of NIR laser irradiation. (c) Viability of TRAMP-C1 cells exposed to ID@PCTPNs with and without acid pretreatment for 24 h in the lack of NIR laser irradiation. (d) Viability of TRAMP-C1 cells receiving ID@PNs with and without acid pretreatment for 24 h in the lack of NIR laser irradiation.

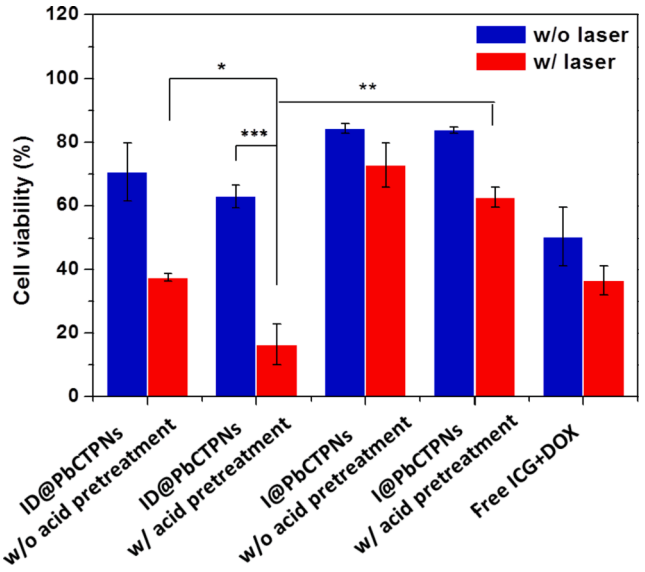

Fig. 8. Cell viability of TRAMP-C1 cells treated with ID@PbCTPNs, I@PbCTPNs and free ICG/DOX mixture with and without NIR laser irradiation (ICG concnetration = 0.4 μM, DOX concentration = 0.63 μM).

pretreatment or not, with NIR laser irradiation, the ID@PbCTPNs showed the superior anticancer capability in suppressing the proliferation of TRAMP-C1 cells as compared to I@PbCTPNs. The results clearly demonstrate that the photothermal/chemo combination therapy of ID@PbCTPNs exposed to NIR irradiation could largely boost the anticancer potency in comparison with single chemotherapy of ID@PbCTPNs in the absence of NIR irradiation and PTT alone of I@PbCTPNs. More importantly, with NIR laser irradiation, the acid-pretreated ID@PbCTPNs displayed significantly augmented cytotoxicity (ca. 84 % cell death) compared to the counterparts without acid pretreatment (ca. 62 % cell death) and free ICG/DOX mixture (ca. 63 % dell death). The findings clearly illustrate the enhancement of anticancer effect from ID@PbCTPNs by means of the increased intracellular concentrations of ICG and DOX molecules upon the promoted cellular uptake and drug release due to their acid-activated PEG detachment.

4. Conclusions

To enhance therapeutic potency of the combined photothermal/chemo therapy by promoting intracellular ICG and DOX delivery, the ID@PbCTPNs equipped with acid-triggered detachable PEG shielding were fabricated by co-assembly of amphiphilic pH-responsive mPEG-b-C_{18}, TPGS hydrophobic PLGA segments, DOX and ICG molecules in pH 8.0 aqueous solution. The angle-dependent DLS and TEM studies showed that the ID@PbCTPNs exhibited a well-suspended spherical

shape. Notably, the ID@PbCTPNs undergoing dePEGylation driven by hydrolysis of benzoic-imine linkers within $mPEG_{5k}$-b-C_{18} in response to pH change from pH 7.4 to 5.0 appreciably accelerated ICG and DOX release. During NIR laser irradiation, compared to free ICG, the ID@PbCTPNs showed superior capability of generating hyperthermia. Moreover, the ID@PbCTPNs dispersed PBS retained outstanding colloidal stability, thereby increasing aqueous photostability of ICG payloads. In vitro cellular uptake and cytotoxicity results suggest that the cellular uptake of ID@PbCTPNs receiving acid pretreatment (at pH 6.5) by TRAMP-C1 cells could be considerably promoted due to acid-elicited dePEGylation, thus boosting their anticancer effect upon the combined photothermal/chemo therapy. Overall, the pH-responsive ID@PbCTPNs featured with superior cellular uptake and intracellular drug release present great promise in enhancing cancer treatment by photothermal/chemo combinatorial therapy.

CRediT authorship contribution statement

Yu-Ning Hung: Conceptualization, Methodology, Investigation, Formal analysis. **Yu-Ling Liu:** Investigation, Validation, Resources. **Ya-Hsuan Chou:** Investigation, Resources. **Shang-Hsiu Hu:** Writing – review & editing, Resources. **Bill Cheng:** Resources. **Wen-Hsuan Chiang:** Conceptualization, Writing – original draft, Writing – review & editing, Supervision, Project administration, Funding acquisition.

Declaration of Competing Interest

The authors declare that they have no known competing financial interests or personal relationships that could have appeared to influence the work reported in this paper.

Acknowledgements

This work is supported by the Ministry of Science and Technology, Taiwan (MOST 107-2622-E-005-008-CC3, MOST 108-2221-E-005-024-MY2 and MOST 110-2628-E-005-001).

Appendix A. Supplementary material

Supplementary data to this article can be found online at https://doi.org/10.1016/j.eurpolymj.2021.110944.

References

[1] X. Yu, X. Tang, J. He, X. Yi, G. Xu, L. Tian, R. Zhou, C. Zhang, K. Yang, Polydopamine nanoparticle as a multifunctional nanocarrier for combined radiophotodynamic therapy of cancer, Part. Part. Syst. Charact. 34 (2017) 1600296.
[2] L. Yu, A. Dong, R. Guo, M. Yang, L. Deng, J. Zhang, DOX/ICG coencapsulated liposome-coated thermosensitive nanogels for NIR-triggered simultaneous drug release and photothermal effect, ACS Biomater. Sci. Eng. 4 (7) (2018) 2424–2434.
[3] J. Deng, F. Liu, L. Wang, Y. An, M. Gao, Z. Wang, Y. Zhao, Hypoxia- and singlet oxygen-responsive chemo-photodynamic Micelles featured with glutathione depletion and aldehyde production, Biomater. Sci. 7 (1) (2019) 429–441.
[4] L. Zhu, P. Li, D. Gao, J. Liu, Y. Liu, C. Sun, M. Xu, X. Chen, Z. Sheng, R. Wang, Z. Yuan, L. Cai, Y. Ma, Q.i. Zhao, pH-sensitive loaded retinal/indocyanine green micelles as an "all-in-one" theranostic agent for multi-modal imaging in vivo guided cellular senescence-photothermal synergistic therapy, Chem. Commun. 55 (44) (2019) 6209–6212.
[5] B. Shrestha, L. Tang, G. Romero, Nanoparticles-mediated combination therapies for cancer treatment, Adv. Therap. 2 (2019) 1900076.
[6] Q.Y. Meng, H.L. Cong, H. Hu, F.-J. Xu, Rational design and latest advances of codelivery systems for cancer therapy, Mater. Today Bio 7 (2020), 100056.
[7] H. Wang, Y. Huang, Combination therapy based on nano codelivery for overcoming cancer drug resistance, Med. Drug Discov. 6 (2020), 100024.
[8] M. Zheng, C. Yue, Y. Ma, P. Gong, P. Zhao, C. Zheng, Z. Sheng, P. Zhang, Z. Wang, L. Cai, Single-step assembly of DOX/ICG loaded lipid-polymer nanoparticles for highly effective chemo-photothermal combination therapy, ACS Nano 7 (3) (2013) 2056–2067.
[9] G. Wei, Y.u. Wang, G. Yang, Y.i. Wang, R. Ju, Recent progress in nanomedicine for enhanced cancer chemotherapy, Theranostics 11 (13) (2021) 6370–6392.
[10] B. Shrestha, L. Wang, E.M. Brey, G.R. Uribe, L. Tang, Smart nanoparticles for chemo-based combinational therapy, Pharmaceutics 13 (2021) 853.
[11] X. Wang, J. Zhang, Y. Wang, C. Wang, J. Xiao, Q. Zhang, Y. Cheng, Multi-responsive photothermal-chemotherapy with drug-loaded melanin-like nanoparticles for synergetic tumor ablation, Biomaterials 81 (2016) 114–124.
[12] C.-C. Hung, W.-C. Huang, Y.-W. Lin, T.-W. Yu, H.-H. Chen, S.-C. Lin, W.-H. Chiang, H.-C. Chiu, Active tumor permeation and uptake of surface charge-switchable theranostic nanoparticles for imaging-guided photothermal/chemo combinatorial therapy, Theranostics 6 (3) (2016) 302–317.
[13] Q. Chen, C. Liang, C. Wang, Z. Liu, An imagable and photothermal "Abraxane-Like" nanodrug for combination cancer therapy to treat subcutaneous and metastatic breast tumors, Adv. Mater. 27 (5) (2015) 903–910.
[14] Z. Gao, W. Mu, Y. Tian, Y. Su, H. Sun, G. Zhang, A. Li, D. Yu, N.a. Zhang, J. Hao, Y. Liu, J. Cui, Self-assembly of paramagnetic amphiphilic copolymers for synergistic therapy, J. Mater. Chem. B 8 (31) (2020) 6866–6876.
[15] X. Wu, J. Liu, L. Yang, F.u. Wang, Photothermally controlled drug release system with high dose loading for synergistic chemo-photothermal therapy of multidrug resistance cancer, Colloids Surf. B Biointerfaces 175 (2019) 239–247.
[16] Y. Yu, Z. Zhang, Y. Wang, H. Zhu, F. Li, Y. Shen, S. Guo, A new NIR-triggered doxorubicin and photosensitizer indocyanine green co-delivery system for enhanced multidrug resistant cancer treatment through simultaneous chemo/photothermal/photodynamic therapy, Acta Biomater. 59 (2017) 170–180.
[17] Z. Gao, Z. Zhang, J. Guo, J. Hao, P. Zhang, J. Cui, Polypeptide nanoparticles with pH-sheddable PEGylation for improved drug delivery, Langmuir 36 (45) (2020) 13656–13662.
[18] L.i. Kong, F. Campbell, A. Kros, DePEGylation strategies to increase cancer nanomedicine efficacy, Nanoscale Horiz. 4 (2) (2019) 378–387.
[19] S. Liu, J. Pan, J. Liu, Y. Ma, F. Qiu, L. Mei, X. Zeng, G. Pan, Dynamically PEGylated and borate-coordination-polymer-coated polydopamine nanoparticles for synergetic tumor-targeted, chemo-photothermal combination therapy, Small 14 (2018) 1703968.
[20] Z. Yang, N.a. Sun, R. Cheng, C. Zhao, Z. Liu, X. Li, J. Liu, Z. Tian, pH multistage responsive micellar system with charge-switch and PEG layer detachment for co-delivery of paclitaxel and curcumin to synergistically eliminate breast cancer stem cells, Biomaterials 147 (2017) 53–67.
[21] N. Guo, Y.i. Zhou, T. Wang, M. Lin, J. Chen, Z. Zhang, X. Zhong, Y. Lu, Q. Yang, D. Xu, J. Gao, M. Han, Specifically eliminating tumor-associated macrophages with an extra- and intracellular stepwise-responsive nanocarrier for inhibiting metastasis, ACS Appl. Mater. Interfaces 12 (52) (2020) 57798–57809.
[22] Y. Fang, J. Xue, S. Gao, A. Lu, D. Yang, H. Jiang, Y. He, K. Shi, Cleavable PEGylation: a strategy for overcoming the "PEG dilemma" in efficient drug delivery, Drug Deliv. 24 (2017) 22–32.
[23] C.-W. Ting, Y.-H. Chou, S.-Y. Huang, W.-H. Chiang, Indocyanine green-carrying polymeric nanoparticles with acid-triggered detachable PEG coating and drug release for boosting cancer photothermal therapy, Colloids Surf. B: Biointerfaces 208 (2021) 112048, https://doi.org/10.1016/j.colsurfb.2021.112048.
[24] N.a. Peng, H. Yu, W. Yu, M. Yang, H. Chen, T. Zou, K. Deng, S. Huang, Y.i. Liu, Sequential-targeting nanocarriers with pH-controlled charge reversal for enhanced mitochondria-located photodynamic-immunotherapy of cancer, Acta Biomater. 105 (2020) 223–238.
[25] T. Yin, Y. Liu, M. Yang, L. Wang, J. Zhou, M. Huo, Novel chitosan derivatives with reversible cationization and hydrophobicization for tumor cytoplasm-specific burst co-delivery of siRNA and chemotherapeutics, ACS Appl. Mater. Interfaces 12 (13) (2020) 14770–14783.
[26] M.C. Xiao, Y.H. Chou, Y.N. Hung, S.H. Hu, W.H. Chiang, Hybrid polymeric nanoparticles with high zoledronic acid payload and proton sponge-triggered rapid drug release for anticancer applications, Mater. Sci. Eng. C 116 (2020), 111277.
[27] A.E. Smith, X. Xu, S.E. Kirkland-York, D.A. Savin, C.L. McCormick, "Schizophrenic" self-assembly of block copolymers synthesized via aqueous RAFT polymerization: from micelles to vesicles, Macromolecules 43 (2010) 1210–1217.
[28] X. Guan, Z. Guo, T. Wang, L. Lin, J. Chen, H. Tian, X. Chen, A pH-responsive detachable PEG shielding strategy for gene delivery system in cancer therapy, Biomacromolecules 18 (4) (2017) 1342–1349.
[29] H. Jin, R. Gui, J. Sun, Y. Wang, Ratiometric two-photon excited photoluminescence of quantum dots triggered by near-infrared-light for real-time detection of nitric oxide release in situ, Anal. Chim. Acta 922 (2016) 48–54.
[30] R. Gui, A. Wan, Y. Zhang, H. Li, T. Zhao, Ratiometric and time-resolved fluorimetry from quantum dots featuring drug carriers for real-time monitoring of drug release in situ, Anal. Chem. 86 (11) (2014) 5211–5214.
[31] Z. Wan, H. Mao, M. Guo, Y. Li, A. Zhu, H. Yang, H. He, J. Shen, L. Zhou, Z. Jiang, C. Ge, X. Chen, X. Yang, G. Liu, H. Chen, Highly efficient hierarchical micelles integrating photothermal therapy and singlet oxygen-synergized chemotherapy for cancer eradication, Theranostics 4 (4) (2014) 399–411.
[32] M. Zheng, P. Zhao, Z. Luo, P. Gong, C. Zheng, P. Zhang, C. Yue, D. Gao, Y. Ma, L. Cai, Robust ICG theranostic nanoparticles for folate targeted cancer imaging and highly effective photothermal therapy, ACS Appl. Mater. Interfaces 6 (9) (2014) 6709–6716.
[33] X. Zheng, F. Zhou, B. Wu, W.R. Chen, D.a. Xing, Enhanced tumor treatment using biofunctional indocyanine green-containing nanostructure by intratumoral or intravenous injection, Mol. Pharmaceutics 9 (3) (2012) 514–522.
[34] C. Zhao, H. Deng, J. Xu, S. Li, L. Zhong, L. Shao, Y. Wu, X.-J. Liang, "Sheddable" PEG-lipid to balance the contradiction of PEGylation between long circulation and poor uptake, Nanoscale 8 (20) (2016) 10832–10842.

[35] Y. Zhang, P. Li, H. Pan, L. Liu, M. Ji, N. Sheng, C.e. Wang, L. Cai, Y. Ma, Retinal-conjugated pH-sensitive micelles induce tumor senescence for boosting breast cancer chemotherapy, Biomaterials 83 (2016) 219–232.
[36] M. Li, Z. Tang, S. Lv, W. Song, H. Hong, X. Jing, Y. Zhang, X. Chen, Cisplatin crosslinked pH-sensitive nanoparticles for efficient delivery of doxorubicin, Biomaterials 35 (12) (2014) 3851–3864.
[37] D. Chang, Y. Gao, L. Wang, G. Liu, Y. Chen, T. Wang, W. Tao, L. Mei, L. Huang, X. Zeng, Polydopamine-based surface modification of mesoporous silica nanoparticles as pH-sensitive drug delivery vehicles for cancer therapy, J. Colloid Interface Sci. 463 (2016) 279–287.